

Full Volume Imaging Gamma-ray Detectors for Enhanced Sensitivity

*K. Ziock, J. Kammeraad, A. Dougan, D. Archer, D.
Beckedahl, J. Blair, D. Knapp, S.J. Luke, and G. Schmid*

March 9, 2001

U.S. Department of Energy

Lawrence
Livermore
National
Laboratory

DISCLAIMER

This document was prepared as an account of work sponsored by an agency of the United States Government. Neither the United States Government nor the University of California nor any of their employees, makes any warranty, express or implied, or assumes any legal liability or responsibility for the accuracy, completeness, or usefulness of any information, apparatus, product, or process disclosed, or represents that its use would not infringe privately owned rights. Reference herein to any specific commercial product, process, or service by trade name, trademark, manufacturer, or otherwise, does not necessarily constitute or imply its endorsement, recommendation, or favoring by the United States Government or the University of California. The views and opinions of authors expressed herein do not necessarily state or reflect those of the United States Government or the University of California, and shall not be used for advertising or product endorsement purposes.

This work was performed under the auspices of the U. S. Department of Energy by the University of California, Lawrence Livermore National Laboratory under Contract No. W-7405-Eng-48.

This report has been reproduced
directly from the best available copy.

Available to DOE and DOE contractors from the
Office of Scientific and Technical Information
P.O. Box 62, Oak Ridge, TN 37831
Prices available from (423) 576-8401
<http://apollo.osti.gov/bridge/>

Available to the public from the
National Technical Information Service
U.S. Department of Commerce
5285 Port Royal Rd.,
Springfield, VA 22161
<http://www.ntis.gov/>

OR

Lawrence Livermore National Laboratory
Technical Information Department's Digital Library
<http://www.llnl.gov/tid/Library.html>

**FULL VOLUME IMAGING GAMMA-RAY DETECTORS
FOR ENHANCED SENSITIVITY
(LDRD Project 98-ERD-025 Final Report)**

*K. Ziock, J. Kammeraad, A. Dougan,
D. Archer, D. Beckedahl, J. Blair, D. Knapp, S. J. Luke, G. Schmid*

Introduction

One of the problems faced by the post-cold-war world is the control of fissile materials. With the deterioration of the command and control structure inside the Former Soviet Union, there is an increased threat that fissile materials will be diverted from a legitimate use to production of weapons of mass destruction by rogue states and or terrorist organizations. The goal of this project was to study and build prototypes of a new class of highly sensitive detectors which could significantly enhance the remote detection of hidden fissile materials. Such an instrument would have a broad applicability in national security applications including nuclear smuggling, arms control, treaty inspections, and safeguards. Additional applications in the non-defense arenas of nuclear medicine, environmental restoration and basic science provide even more reasons to study this technology.

Background

The detection of fissile materials in day-to-day settings, such as ports of entry, requires the use of non-invasive systems which are safe to operate for protracted periods in the presence of the public. This immediately removes active systems from consideration and is one of the primary reasons we chose to focus on detection of the gamma-radiation emitted by fissile materials. This radiation is both ubiquitous from such materials and is sufficiently penetrating that it can be detected remotely through significant amounts of overlying material. The problem with this approach is that the world as a whole emits gamma-radiation which provides a large background on which a small source signal may be present. With the uncertainty as to the type, location--and even presence--of a source, this background makes the problem particularly difficult. It is made even more intractable by the varying nature of the natural gamma-ray background. This can vary by many times itself as a function of location (or possibly as vehicles under inspection transit a choke point). This simple observation means that classic signal-to-noise ratio arguments, based on the use of larger detectors and longer integration times may not apply. Specifically, larger detectors rely on reducing counting uncertainty by collecting more signal. However, when the background varies by order itself, and is unknown *a priori*, more counts may not help one to distinguish this background from true signals included with it. The solution is to collect more information that allows one to separate background from source photons. This can be accomplished by obtaining an image of the world's radiation field and looking for compact sources within this natural diffuse background.

A number of imaging techniques can be applied to this problem, however, due to the penetrating nature of the radiation, they are generally inefficient. To date, systems have relied on proximity, i.e. small detectors scanned in time, collimation or indirect imaging. Collimation severely restricts the field of view of a detector, reducing its sensitivity since it cannot integrate radiation from a passing source or view a wide area if the detector itself is moved. Indirect imaging techniques, such as coded apertures, can improve on this situation but are not optimal in that the

image information is only obtained in an integrated fashion, i.e. all of the data in the detector is used to determine the source strength in each pixel of the image. Hence, the signal to noise ratio can be relatively poor—although there is a very real gain in signal to noise compared to non-imaging systems because a source size determination is generated. What is generally lacking, is a technique which allows one to provide information on the arrival direction of each gamma-ray photon. This technique, widely used at lower energies (i.e. in visible light telescopes or radio antennas) allows one to throw away photons from directions other than the direction of interest so that the noise in a given pixel is determined only by what happens in that pixel. Such systems simultaneously use the whole instrument aperture to collect light into that pixel. At the energies of interest (greater than 100 keV) wide field of view, high efficiency, true imaging modalities do not exist.

A significant improvement over extent systems could be realized if one could efficiently take advantage of the Compton recoil process—the primary interaction mechanism for gamma-radiation with matter over most of the energy range of interest (100 keV to 3 MeV). A Compton imager takes advantage of the fact that gamma-rays can scatter off of the electrons in a detector, depositing some energy at the site of interaction. The amount of energy deposited is a function of the angle through which the gamma-ray scatters. By measuring the location and magnitude of this energy deposition and by measuring the energy and location of capture of the recoiling gamma-ray in another portion of the detector, one can calculate the angle through which the gamma-ray scattered using the Compton formula

$$\cos\theta = 1 - m_0c^2 \left(\frac{1}{E_{\gamma\text{recoil}}} - \frac{1}{E_\gamma} \right) \quad (1)$$

$$E_\gamma = E_{\gamma\text{recoil}} + E_{\text{electron}}$$

referenced to the geometry in Figure 1, where E_i refers to the energy as identified by the subscript i , m_0 , is the rest mass of the electron and c is the speed of light.

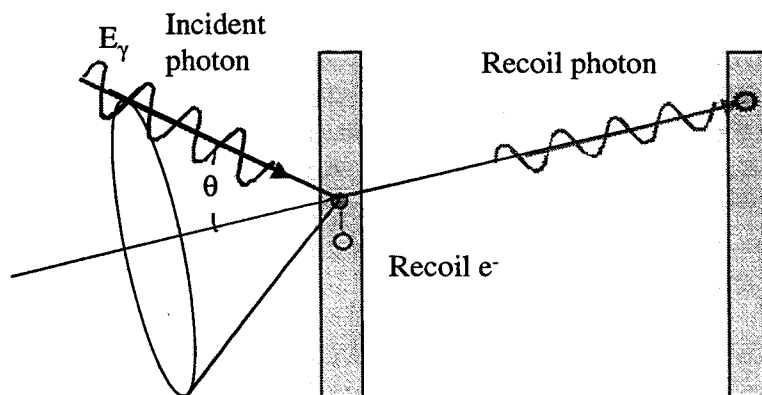


Figure 1. Geometry of a Compton recoil event in a classic two plane detector. Each detector plane measures the x,y location of an interaction and the energy deposited there. The z of the interactions is obtained from the known location of the detector planes.

From the scatter angle, one can determine a ring of directions from which the gamma-ray originated. It is a ring, because one only knows the angle through which the photon scattered from its original direction of travel. To further reduce the ring to a point, would require that one measure the direction that the electron recoiled, which is a more difficult process. Never-the-less, even the ring provides real

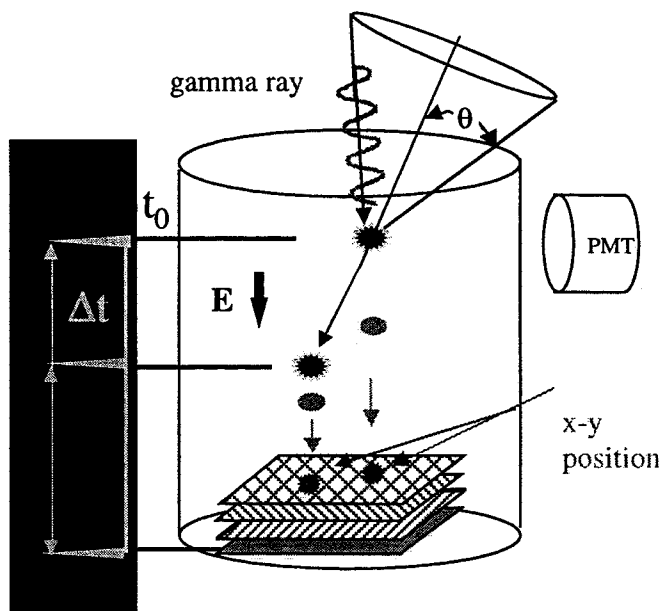


Figure 2. Schematic diagram of a time-projection chamber. At sites of energy deposition, an ionization cloud is generated. Under an applied electric field, the electrons drift at a known velocity to the position-sensitive, readout plane. A prompt scintillation flash at the time of deposition is used to start a timer which is used to determine the z position of the interaction (Schematic plot on the left.) The energy deposited is proportional to the number of electrons collected.

information which can be used to significantly improve the signal to noise ratio in a measurement. The goal of this project was to investigate an improved Compton imager which replaces the classic two plane Compton camera (one plane for the initial scatter detection and one plane for the final photon capture) with a "Full-Volume" detector. Whereas the classic Compton camera measures x, y and energy of each interaction site and infers the separation between the two interactions because they must occur in "thin" planes, the full volume detector provides a large sensitive detector volume which can record, x, y, z and energy for simultaneous energy depositions. This is the information required to fully determine the Compton ring. In addition, with a sufficiently sensitive instrument, one could, also measure the track of the recoiling electron, further reducing the ring to a single direction.

Time Project Chamber Detector

One of the primary selection criteria imposed by our target applications, was to build a large detector capable of intercepting enough of the small number of photons available to achieve a successful detection. The time projection chamber (TPC) is particularly suitable since it can be easily scaled to large sizes since the working medium is simply a noble gas. A schematic diagram of such an instrument is shown in Figure 2. It comprises a large volume (installed size ~ one cubic meter) filled with high pressure noble gas. When a gamma-ray interacts, it produces an energetic electron which produces secondary electrons as it traverses the gas and loses energy. This results in a localized cloud of ionization with the amount of ionization proportional to the energy deposited in the gas. In addition, a prompt flash of scintillation light is produced. This light can be detected with a photo-detector and used to start a timer. An applied electric field is used to cause the electrons to drift, at constant velocity, toward an instrumented readout plane. The time required for the electrons to reach the readout plane is used to determine the z location of the event. The readout plane is designed to both measure the amount of ionization created and the arrival location of the charge. These quantities are used to determine the x, y and energy of the event and when combined with z information allow reconstruction of a Compton ring for the event. In addition, in events with large energy transfer to the original Compton electron (and dependant on the gas pressure, atomic number, and the readout density,) the track of the electron could be recreated to reduce this ring to a single direction. Choice of this detector type was

particularly compelling since all of the subcomponents had been demonstrated in different research fields. For instance, large time projection chambers operated at one atmosphere have been used in the high energy physics community for many years.[1] High pressure gamma-ray spectrometers have been demonstrated at pressures up to 50 atmospheres,[2] although they lack position resolution. Compton imagers have been successfully applied in astrophysical research[3] although these have relied on the classic two plane detector approach and not as a full volume detector. Some effort to bring an entire full volume system together had been performed by the astrophysics community, notably by a group at UCB with the SIGHT instrument[4] which was a gas scintillation proportional imager designed to run at Xe pressures up to 20 atm. and the LXeCAT instrument[5] which is a TPC imager based on liquid Xe which, unfortunately, has poor energy resolution.

At its inception, the project was envisioned as a three year effort with the first year devoted to a design study to understand the system response to various energy gamma-rays. In the subsequent year, this information was to be used to design and build a small prototype chamber. In the remaining time we planned to perform measurements with the system to validate the original calculations. Our ultimate goal was to learn enough about the behavior of such systems to allow design and construction of a full sized prototype—although such a costly undertaking was not envisioned under this funding. The results of each years work are presented below.

Results FY 1998

The primary goals for FY 1998 were to perform a series of simulations which would allow us to design a test-bed detector system. Research questions included understanding design details such as the tradeoffs between gas types, system operating pressure, readout pitch and readout type. In addition, we wished to perform a simulation to fully understand the operational advantages a full-sized system could provide.

To perform these calculations, we turned to established Monte Carlo codes. In particular, GEANT[6] (a detector description simulation tool) from the high energy physics community and EGS[7] (Electron Gamma Shower) codes. These were used to set design goals for the gas pressure and type (i.e. Argon, Krypton or Xenon) vis-à-vis the electron tracking ability.

Our initial question was to understand the conditions necessary to track the Compton recoil electron and reduce the gamma-ray direction of incidence to less than a ring. To successfully track the electron, requires that we establish its direction of travel before it undergoes a

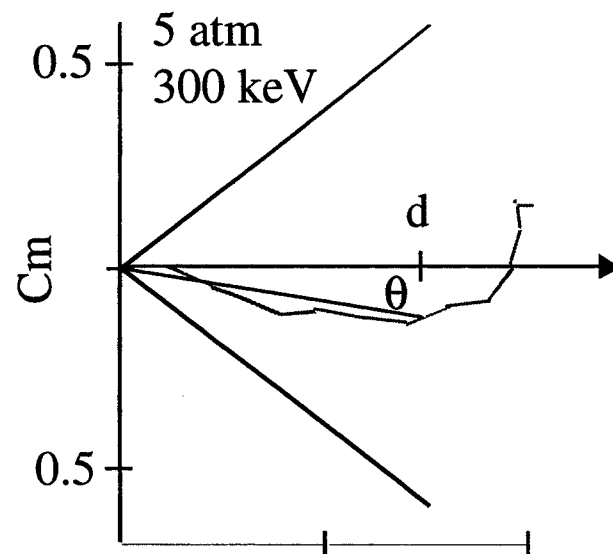


Figure 3. Two dimensional projection of the simulated 300 keV electron trajectory in 5 atm of Argon (in red). At a given distance, d from the starting point we ask what is the total angular deflection, θ , from the original direction of travel.

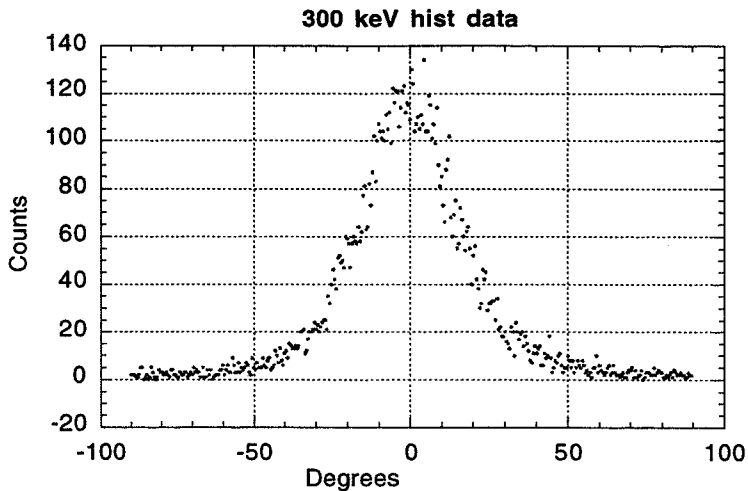


Figure 4. Sample histogram of the electron deflection angle at a fixed distance from the launch point.

was to launch an electron of know energy and trajectory and then see if its total angular deflection, θ , after traversing a distance, d , (see Figure 3) bore any relation to its original direction of travel. This was characterized by creating a histogram of the number of trials versus angular deflection (Figure 4). The width of the histogram represents the degradation of the information content given by the position of the electron at the distance d . Plots of this width as a function of pressure, initial electron energy and gas type provide the information meaningful to simulations of the imaging performance. A sample plot for 300 keV electrons in different pressures of Ar gas is shown in Figure 5. For the simulation conditions used in the figure, it is clear that a significant number of electrons would provide ring area reduction if one achieved a 300 μm readout pitch (distance at the vertical line.)

collision with one of the gas atoms which significantly alters that direction (an event whose likelihood depends on the gas properties.) Rather than try to exactly track each simulated path, we chose to look at two statistics meaningful to the detector readout system and the imaging performance. Since the readout has a finite pitch, the question is really whether the electrons trajectory at the minimum readout spacing still represents its original direction of travel. Our basic approach

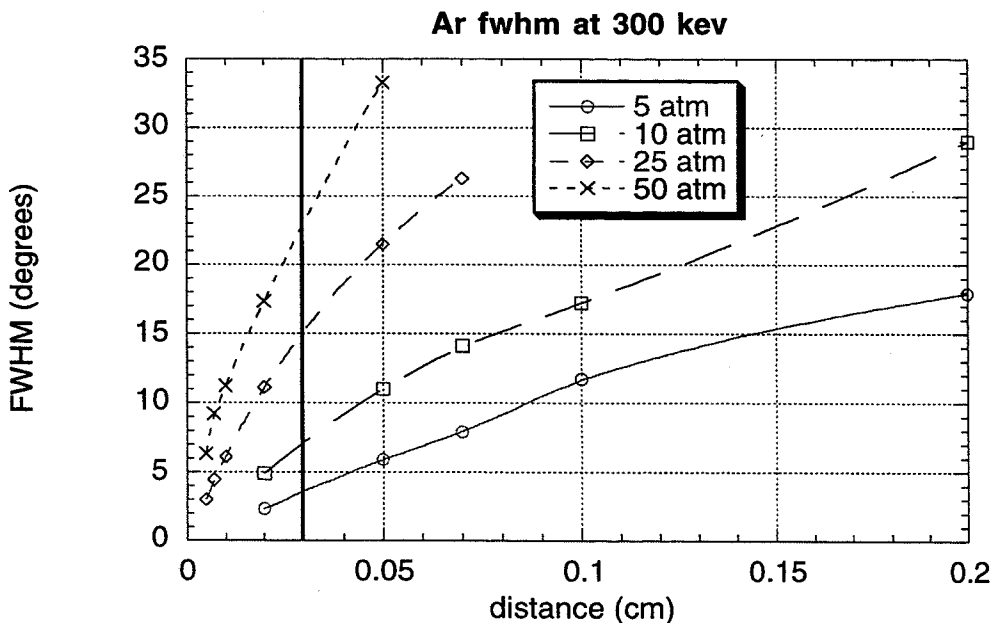


Figure 5. Full width at half maximum of the electron distribution as a function of distance in Argon gas for 300 keV electrons.

To further simplify the result, we went to an even simpler statistic, asking how many of the electrons stay in the same quadrant of space as the original direction of travel in a coordinate system placed at the point of electron release (see Figure 6.) For any electron that stays in the same quadrant, one can reduce the ring to an arc of length 90° . This represents a factor of four reduction in the possible directions of origin. It is important to note that this reduction comes in addition to the factor of 200 already gained from the original Compton ring (see below.)

By comparing results between the two codes (GEANT and EGS), we noted a difference in the answers at the 25% level. Upon further investigation it became clear that neither code is particularly well benchmarked to experimental data at the lower electron energies of interest (~ 100 keV). However, the results are sufficient to show that a position resolution of order $300 \mu\text{m}$ (our target resolution) will allow us to restrict the incident direction of many of the incident photons to less than a full ring.

The optimum detector pitch of $300 \mu\text{m}$ was selected based on an investigation of electron drift in the gas. The limit is set by diffusion of the electrons as they drift from the interaction point to the readout plane over the maximum design distance of 10 cm. This drift occurs under the influence of an applied electric field which must be sufficient to keep the electron-ion pairs, formed at the interaction site, from recombining. The magnitude of the electric field also affects the drift velocity—affecting the time required to readout an event and hence the maximum count rate.

The limit in how far one can drift the charge cloud is provided by gas purity, (the electrons can be trapped by collisions with electro-negative impurity molecules) and by diffusion. Consider that during the course of transit each electron will undergo countless collisions with gas molecules. Between the collisions, it will pick up kinetic energy due to the applied electric field.

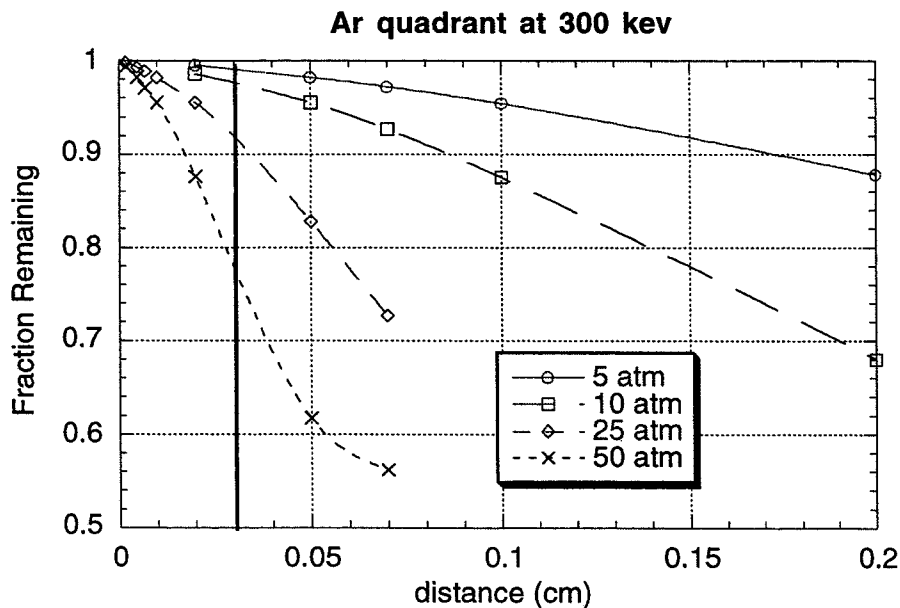


Figure 6. Fraction of 300 keV electrons remaining in the same quadrant as the original direction of travel as a function of distance. Note that at the highest pressures, the drop in fraction remaining at a given distance is primarily due to the fact that the electrons do not reach that distance, rather than that they are in a different quadrant.

If the electron collides elastically with the gas molecule, then it will be deflected sideways, keeping its kinetic energy. This is a particular problem in noble gases since collisions with these remain elastic until the electron has enough energy to excite one of the gas atom electrons (a relatively large amount of energy.) A solution is to introduce a small number of impurity molecules which can absorb the extra kinetic energy so that after a collision the electron just starts drifting in the appropriate direction again. Ideally, one uses a polyatomic gas whose molecules have many closely spaced rotational energy levels. Even small amounts of kinetic energy can be lost from the electron to excite these states.

The 300 μm detector readout pitch was selected to match the diffusion spread for a charge cloud drifting over 10 cm with a suitable polyatomic gas added to the system. Less desirable affects of added gasses include absorption of the UV scintillation photons emitted by the primary noble gas and changes in the ionization properties of the gas. The later is important if charge multiplication is used in an avalanche region to boost the signal size from an event. Final decisions about added gas types were deferred until such time as experiments could be conducted on the effects of the gas.

We also modeled the performance of a full sized detector (one cubic meter in size) to determine an operating gas pressure and type. To this end, we used MCNP to generate photons from a distant point source incident on the detector. Each gamma-ray entering the detector could deposit energy via multiple interactions, including Compton scattering, pair production, and photoelectric absorption. It could also leave the detector with partial or no energy deposition. Secondary processes such as K-fluorescence were also tracked. A list of the interaction history of each photon was saved from MCNP.

The photon interaction file was used as input to a tracking code which mimicked the detector

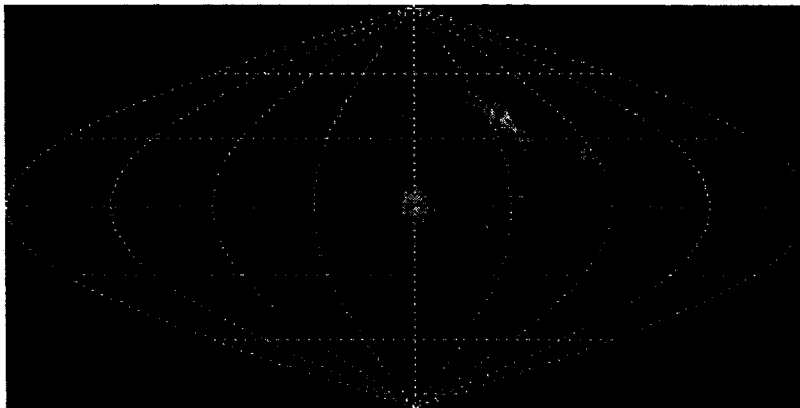


Figure 7. The Compton ring summation process. Each event is accorded a unit probability which is distributed on a ring of Gaussian profile given by the angular uncertainty. The probability is weighted to the pixels in the θ vs. $\Phi\sin\theta$ plot format which shows all of 4π . Where rings overlap, the probabilities add. In this image three events are shown with Gaussian widths increased an order of magnitude from calculated levels to better illustrate the process. (Probability increases from black to yellow.)

response. Using an assumed inability to distinguish separate energy deposition sites closer than 500 μm , such depositions were combined as one using an energy/separation weighting technique. The resulting interaction list was then searched for energy depositions commensurate with K-shell fluorescence using energy windows based on published energy resolution values. These were attributed to the nearest non-fluorescence energy deposition. The process resulted in a list of energy deposition sites each having x, y and z coordinates and an energy of

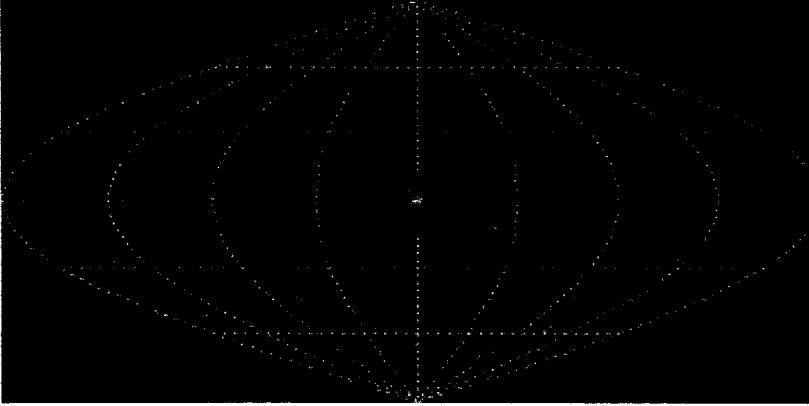


Figure 8. False color "image" of a point source (center) with 25 detected counts in a 300 count background. The θ vs. $\Phi \sin\theta$ plot format shows all of 4π .

initial scatter (i.e. which occurs first.) In this case, two Compton rings with appropriate widths were generated. The code output a list of events with ring and error sizes.

The output ring data was used by another code which generated a false color image of the rings on a θ vs. $\Phi \sin\theta$ plot as shown in Figure 7. The ring from each photon was given a unit probability which was distributed based on the diameter of the ring and on a Gaussian profile based on the width from the error analysis, i.e. each ring would look similar to a "fuzzy" doughnut. This probability map was then transformed to the pixels of the θ vs. $\Phi \sin\theta$ plot, maintaining the total probability of the ring. The process is shown for three photons of exaggerated error width (ten times the calculated values) in Figure 7. As can be seen, where rings overlap, the probability of the rings adds to show more probable source locations.

The results from a full simulation are shown in Figures 8 and 9 where only 25 source gamma-rays clearly show the presence of the source against a uniform background of 300 gamma-rays. A traditional, omni-directional detector would require 13 times as long to achieve a very marginal 5 sigma detection (and *only* if one knew what the background levels were to begin with.)

From simulations of this type, an efficiency and fractional ring area were calculated for the detector as a whole. The former is just the fraction of the incident photons which provide a meaningful Compton ring. The latter is the average ring area determined from all events divided by 4π and tells how much background the system can reject at that

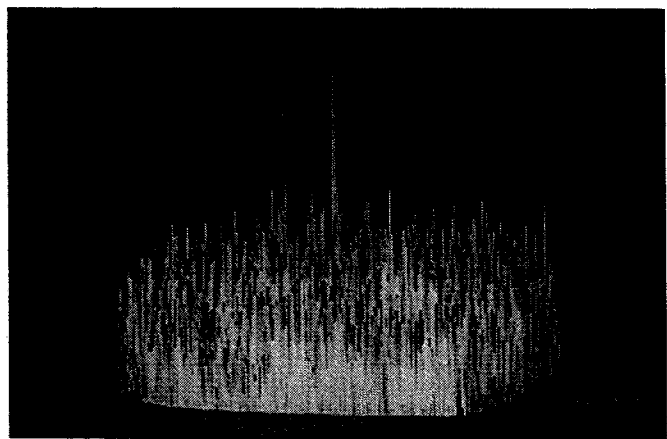


Figure 9. Same data as in Fig. 8 but as a surface plot. The source (center) is clearly seen to stand out above the noise.

deposition. These were searched to find an order of occurrence commensurate with the Compton formula (1). If a successful ordering was found, a Compton ring was calculated. The width of the ring was also calculated based on simple error propagation using expected energy and position uncertainties. Note that for higher energy events, one cannot always uniquely determine which vertex of a pair represents the site of

Table 1
Detector Performance at Different Energies

Gamma-ray energy	Fractional Ring Area	Quantum Efficiency
511 keV	0.4%	50%
1 MeV	0.3%	30%
1.8 MeV	1.2%	20%

energy. The results at several energies are presented in Table 1. However, it should be noted that the highest energy work (1.8 MeV) did not correctly handle pair production events, which reduced its perceived performance.

During the latter half of the year we started to use these results to design an experimental system which was to be constructed in the second year of the project.

Results FY 1999

For the second year of the project, the TPC effort was combined with a separate, on-going research program to create a portable, Full-Volume detector using germanium as the detector material.[8] The decision to combine the two programs was based on the similar approaches to gamma-ray detection. The Compton imaging principles behind the germanium Full-Volume detector are the same as those for the noble gas detector system. The gains in performance over extent, non-imaging and indirect imaging detectors are also similarly compelling. Finally, the target community for the two programs was the same, although, due to the difference in detector sizes, the instruments address complementary regions of programmatic need. Whereas the germanium system, based on a single coaxial detector, is intrinsically portable, the one cubic meter of the gas system provides enhanced sensitivity for fixed and vehicle mounted applications.

The Germanium imager is based on a coaxial detector with the outer electrode segmented to provide multiple readout locations (see Figure 10.) The position of an event is determined by processing the different time digitized signals from the electrodes. These record not just the magnitude of the energy deposition (as is recovered in a normal instrument) but also the time history of the drift of the electrons and holes. As the electron-hole charge cloud is generated and pulled apart by the applied electric field in the detector, the charge carriers induce a signal on the inner and outer electrodes. This signal increases as the carriers come near an electrode and reaches a steady state on those electrodes which actually collect charge. On the neighboring (or spectator) electrodes, the induced signal will return to zero as the charge is collected by the "home" electrode. Radial information is encoded in the shape of the time record of the home electrode, while azimuthal and longitudinal information is obtained by comparing the size of the induced signal in the neighboring electrodes. This comparison allows one to use relatively large electrodes compared with the ultimate position resolution. A technique which greatly reduces the complexity of the instrument.

FY 1999 represented the third and final year of LDRD funding for the germanium imager. In previous years, the project had completed extensive simulations of the behavior of a segmented detector based on signals measured on a classic (non-segmented) contact detector. The goal in FY 1999 was to perform measurements on a segmented detector which was being developed for

nuclear physics experiments at LBNL known as the GRETA (Gamma-ray Energy Tracking Array) prototype.

FY 1999 represented the third and final year of LDRD funding for the germanium imager. In previous years, the project had completed extensive simulations of the behavior of a segmented detector based on signals measured on a classic (non-segmented) contact detector. The goal in FY 1999 was to perform measurements on a segmented detector which was being developed for nuclear physics experiments at LBNL known as the GRETA (Gamma-ray Energy Tracking Array) prototype.

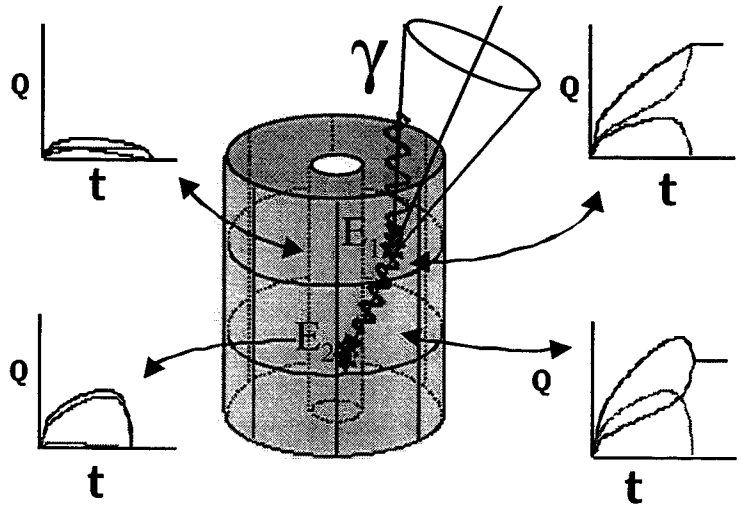


Figure 10. Schematic diagram of the coaxial germanium, Full-Volume detector. Different signals expected from the different electrodes (shown on the small graphs) are used to find the location of multiple simultaneous energy depositions.

Germanium Imager results

As mentioned in the preceding paragraph, the primary goal of the germanium detector portion of the project was to perform position resolution measurements on a segmented detector. Preliminary arrangements had been made with the LBNL group working on the GRETA detector to pursue such measurements and were scheduled to commence early in the fiscal year.

Unfortunately, this work was delayed when the manufacturer was (ultimately) ~ 1/2 year late in delivering the prototype segmented detector.

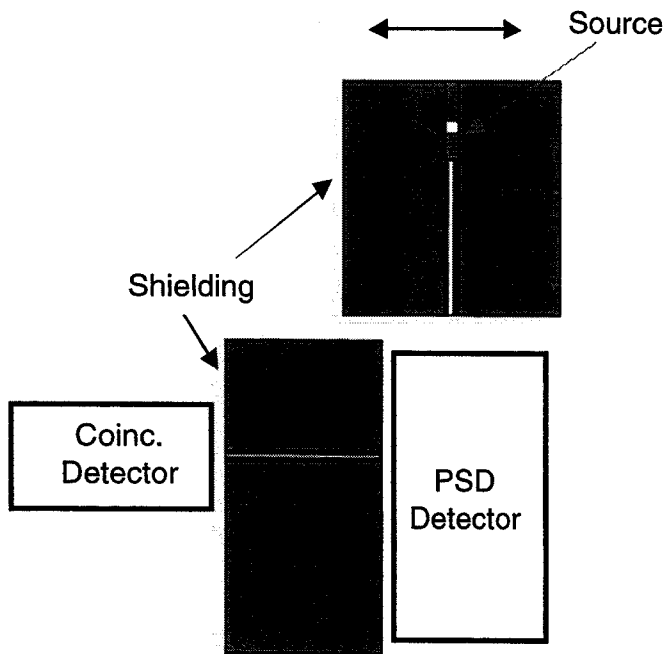


Figure 11. Schematic diagram of apparatus used to test detector position resolution in the position sensitive detector (PSD.)

To aid in developing the techniques we planned to use on the GRETA detector once it arrived, we undertook similar measurements on a commercial, coaxial detector to verify the radial position resolution of the technique. To determine the position resolution required the ability to deposit a known amount of energy at a known location within the detector. The Compton scatter process was selected to achieve this. A schematic of the measurement geometry is shown in Figure 11. A collimated ^{137}Cs source was positioned to send a beam of gamma-rays into the end of the position sensitive detector. A

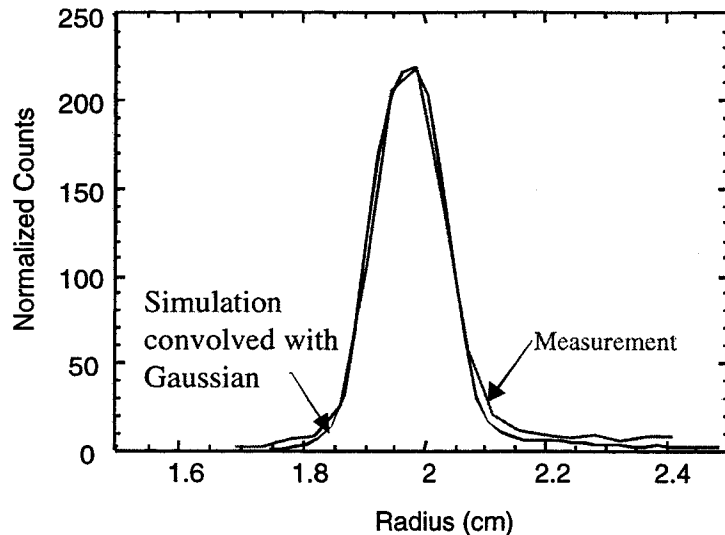


Figure 11. Radial distribution of events measured in a commercial coaxial detector. The derived position resolution is 400 μm .

determined in previous years. For a given source location, a histogram of the number of events versus measured radius was generated. To determine a detector position resolution required that we account for the width of the gamma-ray beam as defined by the collimator. This was determined using a Monte Carlo model of the experimental setup. The simulated results were then fit to the measurement with inclusion of a convolved Gaussian to represent the measurement width. A one sigma result of 400 μm was obtained!

An additional result from this series of measurements was to map the charge carrier drift velocity at different locations on a concentric circle of the detector (Figure 12). The variation in this number occurs as the drift direction changes with respect to the crystal axis of symmetry. The magnitude of the number is important because it affects the position determination in a fully segmented system where the event location is not known *a priori*. The results shown in Figure 12 agree with published values in the literature and indicate that the center of our circle was offset by 1 mm from the detector center!

The GRETA prototype did finally arrive and measurements on a fully segmented system were undertaken. A sample of the data collected is shown in Figure 13. Due to the late start of the measurements, analysis of the results extended beyond the end of the fiscal year. Details can be found in reference [9].

Gas Detector Progress

Our goal for the time projection chamber project was to build and turn on an experimental facility to

second germanium detector, behind a slit collimator at right angles to the beam, looked at the scattered radiation from a small volume element of this beam. A coincidence between the two detectors was used to indicate that a Compton scatter had occurred and energy cuts were used to restrict the geometry to a single scatter in the desired volume. The location of deposition could be moved by translating both the source and its collimator, which were mounted on a translation stage.

The data collected from this system was processed using the algorithms

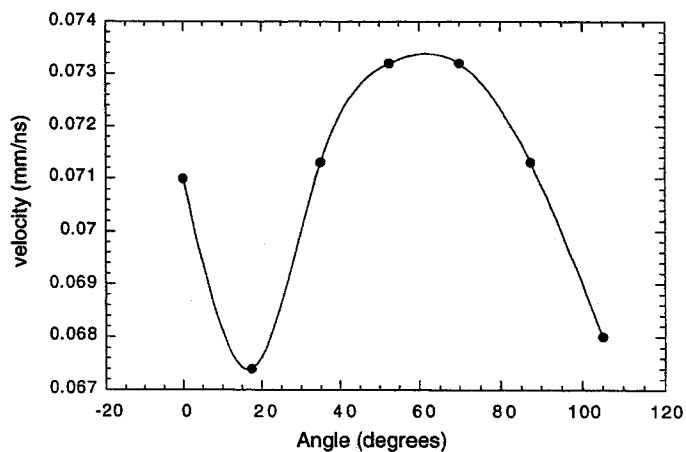


Figure 12. Carrier drift velocity as a function of detector azimuth. The asymmetry in the results can be explained if a one millimeter offset between the detector and measurement centers is introduced.

test the results of the calculations performed in the preceding year. There were two major concerns in the construction of the system. The first and primary concern centered on the gas purity. Reports in the literature[10] indicated gas purities at the parts per billion level were required to successfully drift the electrons generated at the interaction sites to readout planes a few centimeters away. This extreme sensitivity to gas purity at high pressures can be qualitatively understood in the increased number of collisions between the drifting electrons and gas molecules. If one of the gas molecules struck is an electronegative impurity such as oxygen, it will grab the electron, effectively removing it from the collection process. In cases of moderate contamination this leads to a change in the charge collected as a function of drift distance, in cases of severe contamination no signals may be seen except from areas immediately adjacent to the readout system. To achieve this level of purity requires that the system design is "clean," i.e. contains no materials which out gas electronegative materials and that the gas can be cleaned in the system. In addition, by this time it was clear that xenon was the gas of choice because of its higher atomic number (and therefore higher stopping power for the gamma-rays.) Unfortunately, xenon is very expensive so a means to recover and store gas from the experimental chambers

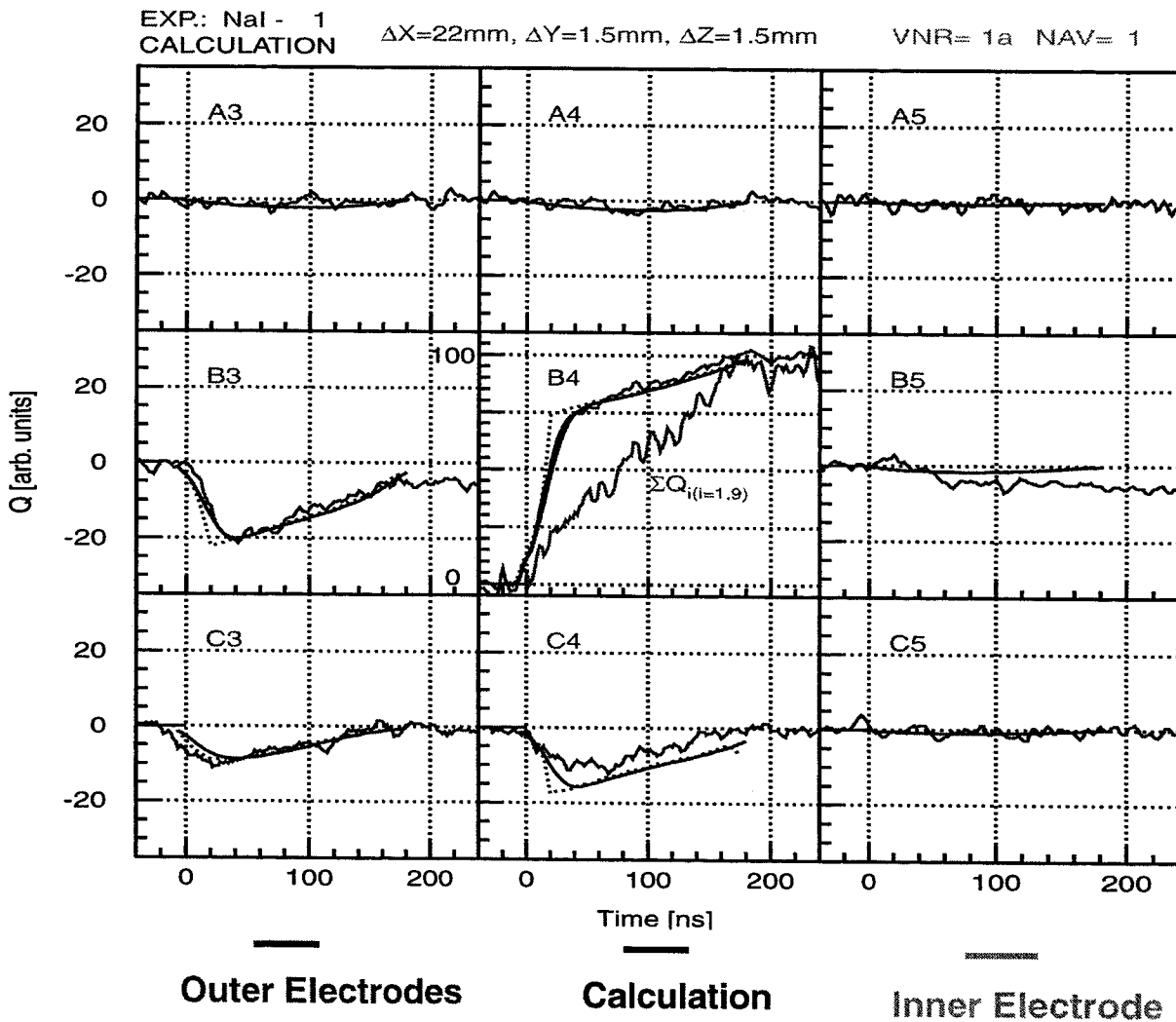


Figure 13. Sample event obtained with the GRETA detector showing the home electrode response (center) and that of the neighboring nine spectator electrodes.

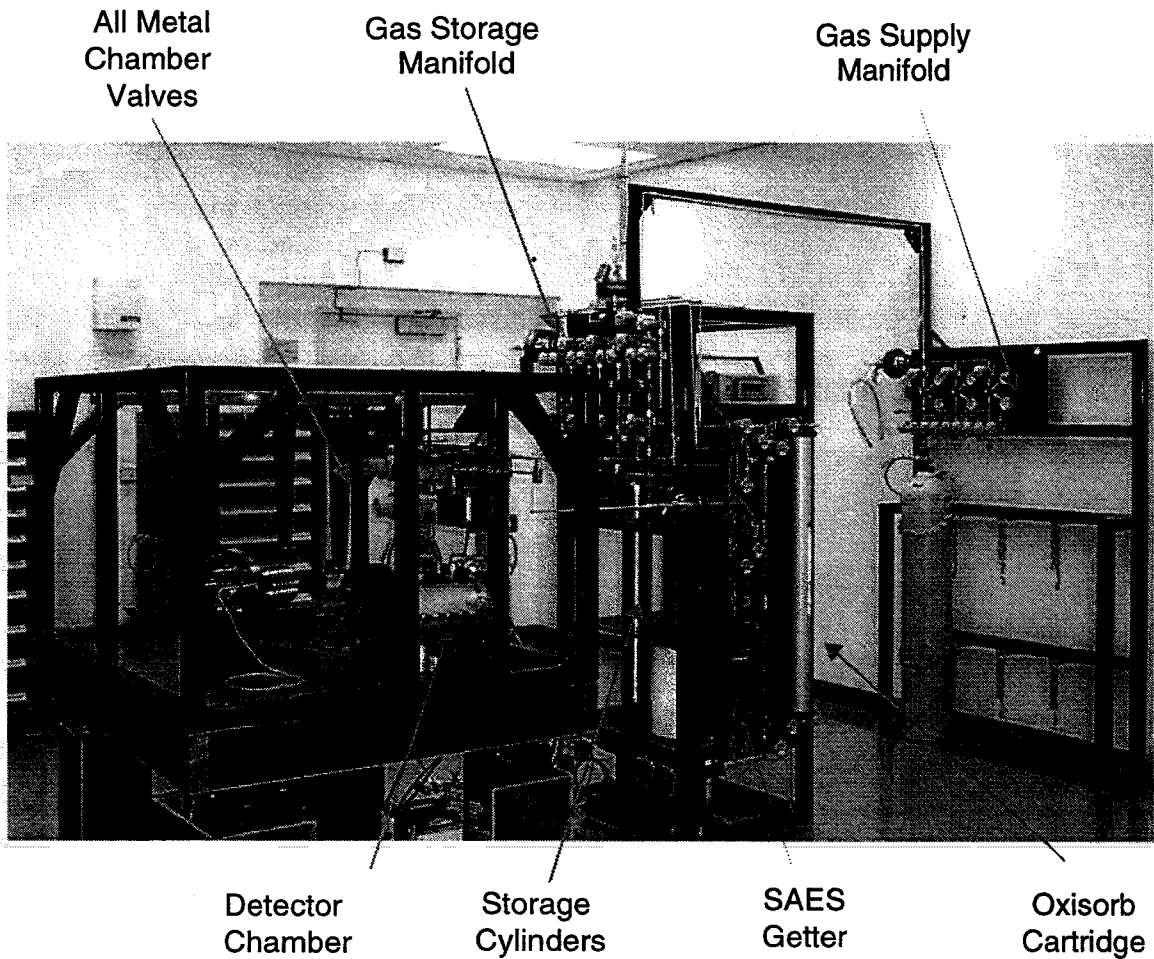


Figure 14. Photograph of the time projection chamber experimental system.

was absolutely essential.

An additional concern centered on building a versatile experimental station which was certified to operate at pressures up to 50 atmospheres. This required careful design of the detector housings to provide maximum flexibility while still meeting laboratory ES&H concerns.

In the end, we contracted out construction of the gas handling system based on our design specifications, since the purity requirements in the local semiconductor industry were similar to ours (although the contaminant list differed.) The experimental chambers were designed and constructed in house. A total of two chambers were built to

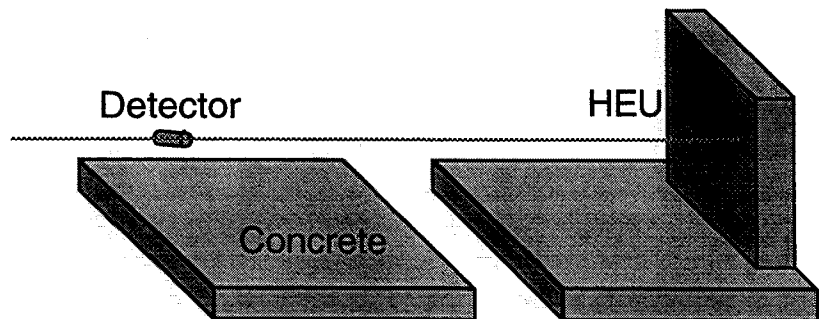


Figure 15. Simulation geometry with a highly enriched uranium (HEU) source and a full-volume Ge detector. The three dimensional concrete structure is itself a source of radiation.

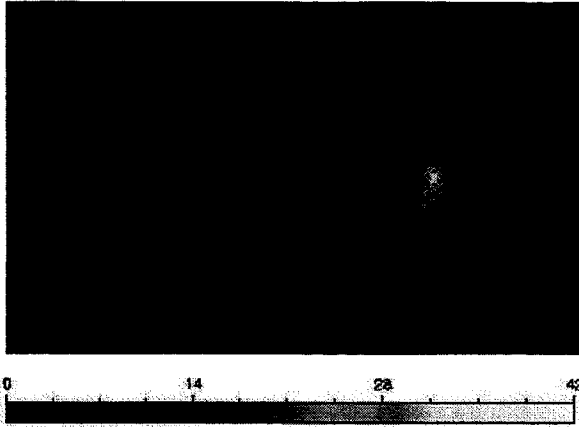


Figure 15 Simulation with Ge detector based on the geometry in Fig. 14. The image is made using only gamma-rays with 186 keV.

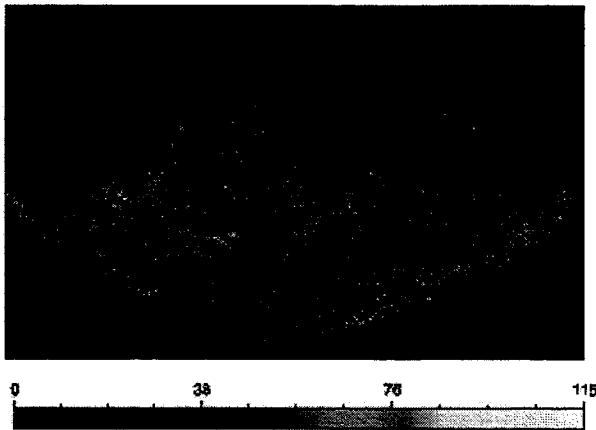


Figure 16. Simulation with Ge detector based on the geometry in Fig. 14. The data is made using the 1461 keV background line from the concrete in the simulation

year to complete, with the final pressure tests of the installed system occurring shortly before the close of the fiscal year.

Modeling Program

In support of both experimental programs, we continued our modeling efforts at a low level (due to budgetary constraints.) In particular, we addressed the unique opportunity a full-volume imager will provide to map the gamma-ray background of the world. Previous work at the laboratory had shown that the background varies on order many times itself and can do so on distance scales relative to the field of view of one of our detectors. It is against this variable "clutter" that our detectors must be able to see point sources. To start on understanding the structures we are likely to see, we set out to model the background structures.

reserve one for experimental work while the other could be used to purify the gas with a titanium dust generator and or to conduct gas purity measurements.

The system is shown in Figure 14 and comprises a gas input manifold suitable for adding both noble and impurity gasses, a two-step gas cleaning system, a mass flow controller, two experimental chambers, four gas recovery cylinders and the various valves and piping required to interconnect the components. To move gas through the system cryogenic techniques were selected. The recovery cylinders were designed to allow immersion in liquid nitrogen which liquefies the xenon, effectively sucking it out of other portions of the apparatus. The chambers also have cold fingers which can be immersed in liquid nitrogen to allow pressurization of the chambers beyond the 100 psi rating of the gas cleaner elements. To run the system with the cryogen, the quantity of gas collecting in a chilled portion of the apparatus is carefully monitored using the mass flow controller. When the preselected gas mass (which will give a desired pressure on reaching room temperature) has transferred, the cold part of the system is sealed and allowed to warm up while the pressure is monitored.

Design, construction, installation and certification of the components required the full

The first step was to accurately generate the radiation emitted by background materials. We chose concrete as a first example. A realistic radiation model of concrete was generated based on the known primordial U(4 ppm) and Th (12 ppm) concentrations in the Earth's crust. This was allowed to age to asymptotic equilibrium (~ 6 million years) and an arbitrary amount of ^{40}K added to the mix. The radiation from the resultant radio-isotopes was propagated through normal concrete constituents to arrive at a fully Comptonized spectrum. The results were sent through a detector response model for comparison to the measured spectrum taken inside a concrete structure with a germanium spectrometer. Agreement within a factor of two was obtained over the entire spectral band from 100 keV to 3 MeV. This material was then used to create a three dimensional structure as shown schematically in Figure 14. A source of highly enriched uranium was placed at one end of the simulation with a Full Volume germanium detector at the other end. The results are shown in Figures 15 and 16. The source is clearly visible against the background.

FY 2000

FY 2000 represented the last year of funding for this program. The primary goal was to demonstrate Compton imaging in the laboratory prototype time projection chamber constructed in FY 1999. Numerous secondary goals included verifying calculations made in the first year of the project by varying experimental conditions. The germanium portion of the project was phased out since it had already received three years of funding.

Progress was severely hampered by the funding allocation which, due to the general LDRD cuts imposed by Congress, was less than half of the requested amount. Based on the funding levels, the goals for the project were curtailed to simply demonstrating Compton imaging at modest pressures. However, to allow for transition to programmatic funding and the federal proposal cycle, the timeline was set aggressively to achieve this by early Spring of 2000. Unfortunately, this left no contingency in either the schedule or the budget to allow for the inevitable setbacks which arise in an experimental program. We encountered an immediate setback in procuring a patterned readout plane for the detector, its cost and delivery changing by a factor of two from estimates we had obtained from the relevant parties in the previous year. Worse, the work would only be on a best effort basis with estimated chances of success at 60%. None of these were compatible with our extremely tight resources.

Against this developing crisis, we proceeded to test the system as planned, using it as a simple ionization chamber (see Figure 17) to check gas purity. Scintillator paddles were placed on either end of the chamber and set to trigger the data acquisition system if both fired simultaneously. This signal indicated passage of a minimum ionizing charged particle through the chamber which should deposit a

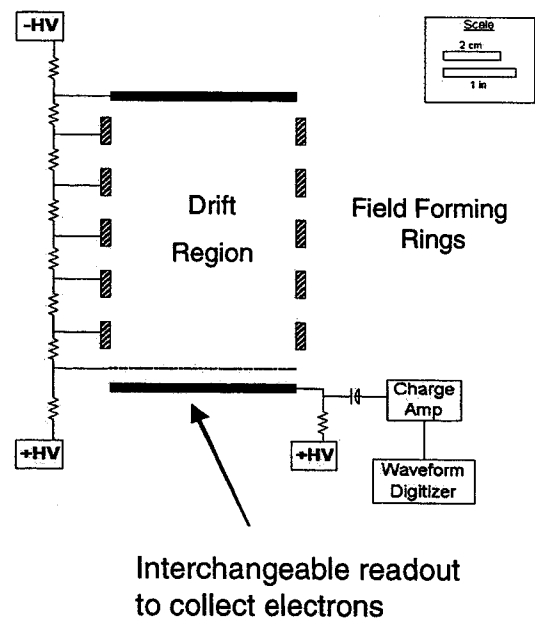


Figure 17. Schematic diagram of the detector showing a drift region enclosed by field forming rings. Between the drift region and the interchangeable readout is a grid to allow increasing the electric field in between the grid and the readout plane to achieve gas gain.

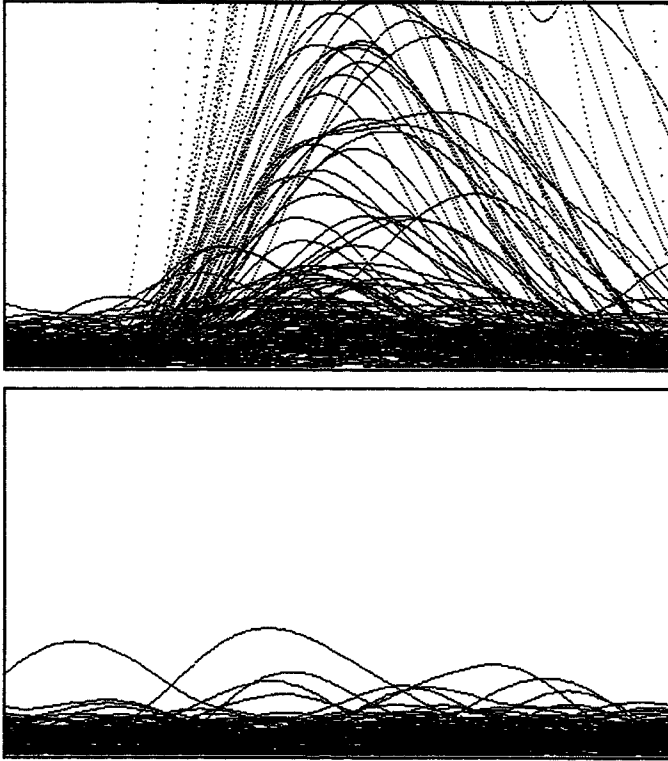


Figure 18. First signals seen from the TPC. The horizontal axis is time (total length 81.76 μ S), and the vertical axis represents amount of charge collected. The upper data is taken using the scintillator paddle trigger described in the text. The bottom data is triggered at random. Although tracks are clearly seen, the expected uniform trace height does not exist.

University of Louisville which had developed microwell detectors patterned on a plastic substrate for use in space based applications.[11] Although we were concerned about gas purity with this substrate, it was clear this would not be an issue at the more modest pressures that we could hope to achieve with our restricted resources. When we received sample readout planes from the group, we were unable to keep them from sparking, a problem which had also plagued our multi-wire work. This problem was finally localized to one of the two gas purifiers, which was apparently adding fine particulates to the gas. When we bypassed this element, we were able to achieve the voltage conditions needed to create gas gain in the system and successfully recorded some gamma-ray spectra with the microwell readout. A sample spectrum from a ^{133}Ba source is shown in Figure 20. The two peaks

fixed energy in the system. The idea was to digitize the signal and check for gas purity by verifying that tracks could be detected from the entire length of the drift chamber. Unfortunately, the signals from the chamber, while clearly showing the charged particles were detected, did not show the uniform size needed to proceed with the gas purity tests (Figure 18).

To obtain a signal of fixed amplitude, we proceeded to illuminate the chamber with a collimated gamma-radiation source. Again, although detected, the signals were too small to produce a meaningful spectrum without gas gain. To generate gas gain, we replaced the plate anode with a multiwire anode. Although this tended to spark before sufficient gains could be achieved, when they were achieved, a good spectrum was not obtained (Figure 19.)

To realize a viable readout, we abandoned our efforts to procure one made to our own specifications. Instead, we started to work with a group at the

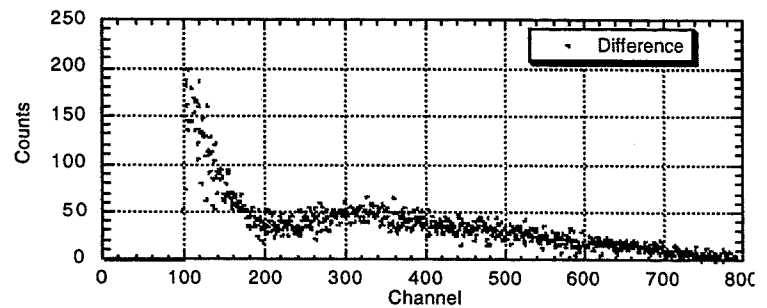


Figure 19. Gamma ray "spectrum" obtained with ^{133}Ba source. The chamber is run with multiwire anodes and gain. No spectral features are present in the data to allow for system calibration.

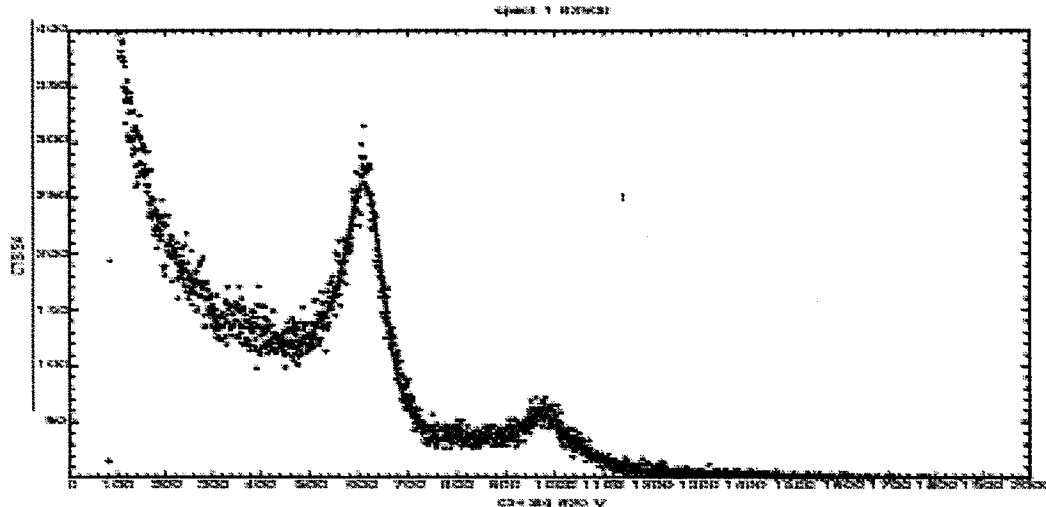


Figure 20. ^{133}Ba spectrum taken with the system at 1.6 atm Xe with the microwell detector. The high energy peak is identified with the 81 keV radiation from the source, the lower energy peak is identified as the K-fluorescence escape peak from this line. Due to the small volume of the active area of the detector ($\sim 2 \times 2$ cm) the escape peak is much larger than the primary peak.

represent the 81 keV line from the source and the K-shell fluorescence escape peak(s) at ~ 51 keV. By running this at multiple voltages we are able to obtain the expected exponential relationship between the voltage and the signal gain as shown in Figure 21. These results clearly indicate that the system is functioning as a gamma-ray detector, although position resolution remains to be demonstrated.

Conclusions

The realization of a full-sized, Full-Volume, gamma-ray imager was never the goal of this LDRD program. Rather, our goal was to demonstrate a small working prototype suitable to test the physical ideas behind such an instrument, before this more costly undertaking was started. This work continues today.

For the gas system we realized our goal of a working test bed, however this took all of our resources leaving much of the experimentation yet to be performed. We have received funding to start studying some of the open issues such as readout design. More importantly, we found no technical obstacles that indicate a large Full-Volume imager cannot be built. In fact, the simulations conducted early in the program clearly indicate the value of such an instrument with its 200:1 background rejection based solely on gamma-ray trajectories derived from classic Compton imaging. These simulations hold for the germanium imager as well. The results obtained in the final year of LDRD funding for that project were sufficient to obtain programmatic funding to build a prototype optimized for imaging applications.

References

1. See e.g. F. Sauli and A. Sharma, Annual Review of Nuclear and Particle Science **V49**, 341-388, 1999.
2. K. Vlasik, et al. Instruments and Experimental Techniques, **V42**, 685-693, 1999.
3. V. Schonfelder, et al., Astrophysical Journal Supplement Series, **V86** N2:657-692, 1993.
4. J. Wilkerson, et al. IEEE Transactions On Nuclear Science **38**(2): 580-584, 1991.

5. E. Aprile, et al., Astronomy & Astrophysics Supplement Series **120**(4 SI): C649-C652, 1996.
6. R. Brun, et al., GEANT3 users' guide, DD/EE/84-1, CERN (1987). R. Brun, et al., GEANT3 users' guide, DD/EE/84-1, CERN, 1987.
7. The code and information may be obtained from, "<http://ehssun.lbl.gov/egs/egs.html>"
8. J. Kammeraad, et al, "Innovative Uses for Conventional Radiation Detectors via Pulse Shape Analysis," UCRL-ID-133563, LLNL, 1999.
9. K. Vetter, et al., Nuclear Instruments and Methods in Physics Research **A452**, 223-228, 2000.
10. E. Aprile, M. Suzuki, IEEE Transactions on Nuclear Science **36**, 311-315, 1989.
11. W. Pitts, et al., Nuclear Instruments and Methods in Physics Research **A438**, 277-281, 1999.

This work was performed under the auspices of the U.S. Department of Energy by the University of California, Lawrence Livermore National Laboratory under Contract No. W-7405-Eng-48.